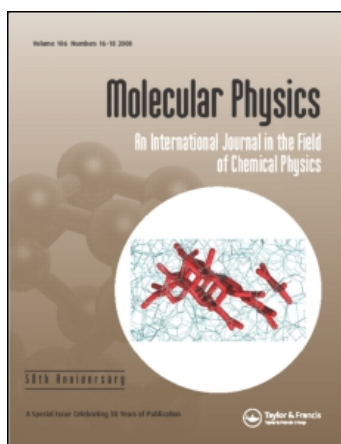


This article was downloaded by: [CDL Journals Account]
On: 20 November 2008
Access details: Access Details: [subscription number 786945879]
Publisher Taylor & Francis
Informa Ltd Registered in England and Wales Registered Number: 1072954 Registered office: Mortimer House,
37-41 Mortimer Street, London W1T 3JH, UK



Molecular Physics

Publication details, including instructions for authors and subscription information:
<http://www.informaworld.com/smpp/title-content=t713395160>

Photoelectron-photofragment angular correlations in the dissociative photodetachment of HOCO^-

Zhou Lu ^a; Jonathan E. Oakman ^a; Qichi Hu ^a; Robert E. Continetti ^a

^a Department of Chemistry and Biochemistry, University of California, California 92093-0340, USA

Online Publication Date: 01 January 2008

To cite this Article Lu, Zhou, Oakman, Jonathan E., Hu, Qichi and Continetti, Robert E.(2008)'Photoelectron-photofragment angular correlations in the dissociative photodetachment of HOCO^- ',Molecular Physics,106:2,595 — 606

To link to this Article: DOI: 10.1080/00268970801971376

URL: <http://dx.doi.org/10.1080/00268970801971376>

PLEASE SCROLL DOWN FOR ARTICLE

Full terms and conditions of use: <http://www.informaworld.com/terms-and-conditions-of-access.pdf>

This article may be used for research, teaching and private study purposes. Any substantial or systematic reproduction, re-distribution, re-selling, loan or sub-licensing, systematic supply or distribution in any form to anyone is expressly forbidden.

The publisher does not give any warranty express or implied or make any representation that the contents will be complete or accurate or up to date. The accuracy of any instructions, formulae and drug doses should be independently verified with primary sources. The publisher shall not be liable for any loss, actions, claims, proceedings, demand or costs or damages whatsoever or howsoever caused arising directly or indirectly in connection with or arising out of the use of this material.

RESEARCH ARTICLE

Photoelectron-photofragment angular correlations in the dissociative photodetachment of HOCO^-

Zhou Lu, Jonathan E. Oakman, Qichi Hu and Robert E. Continetti*

Department of Chemistry and Biochemistry, University of California, San Diego,
9500 Gilman Drive, La Jolla, California 92093-0340, USA

(Received 16 October 2007; final version received 23 December 2007)

A coincidence study of the photoelectron-photofragment angular distributions in the one- and two-photon dissociative photodetachment (DPD) of HOCO^- is reported. The photoelectron angular distributions in the one-photon DPD channels $\text{HOCO}^- + h\nu \rightarrow \text{OH} + \text{CO} + e^-$ and $\text{HOCO}^- + h\nu \rightarrow \text{H} + \text{CO}_2 + e^-$ at $E_{h\nu} = 3.21$ eV are examined in both the laboratory and neutral photofragment recoil frames, while the angular distributions of the OH + CO products in the laboratory frame are also investigated. The results show a parallel dipole transition for the DPD of HOCO^- . The radical lifetime was examined as a function of the orientation of the transition dipole, with upper limits of 9×10^{-13} s and 1.3×10^{-12} s estimated for HOCO and DOCO lifetime for dissociation into OH/OD + CO, respectively. The photoelectron-photofragment angular correlation in the two-photon DPD of HOCO^- is also presented, showing that when the photon energy is near the photodetachment threshold, a molecular anion like HOCO^- can be effectively aligned through a continuum shape resonance.

Keywords: dissociative photodetachment, recoil-frame photoelectron angular distribution

1. Introduction

Dissociative photodetachment (DPD) of negative ions has become a unique and versatile tool for the study of the dynamics of gas-phase transient species [1,2]. In a typical DPD process, electrons are photoejected from parent anions, producing neutral transient species that can further dissociate into two or more photofragments. A coincidence measurement of the translational energy partitioning among photoelectron and photofragments from the same DPD event can yield deep insight into the dissociation dynamics on the involved potential energy surfaces (PES) [1,3]. Complementary to the recording of energy partitioning, the measurement of photoelectron and photofragment angular distributions is another powerful probe of the DPD dynamics [3–5]. In this work, we extend such measurements to the HOCO^- and DOCOCO^- molecular anions previously used to probe the $\text{OH} + \text{CO} \rightarrow \text{H} + \text{CO}_2$ reaction [6,7].

Under the electric-dipole approximation, the photodetachment probability is dictated by:

$$I \propto |\langle \varphi_{ele} \cdot \varphi_f | \vec{\mu} \cdot \vec{E} | \varphi_i \rangle|^2 = |\vec{M} \cdot \vec{E}|^2, \quad (1)$$

where $\vec{\mu}$ is the dipole moment operator, \vec{E} is the laser electric field, φ_{ele} , φ_f , and φ_i are the wave-functions of the free electron, the neutral products, and the parent anion, respectively, and $\vec{M} = \langle \varphi_{ele} \cdot \varphi_f | \vec{\mu} | \varphi_i \rangle$ is the transition dipole moment. In general, parent anions are isotropically distributed before interacting with the photons, while the laser polarization is spatially fixed and defines the laboratory frame (LF). The transition dipole moment has a specific direction in the molecular frame (MF). As a result, based on Equation (1), the angular distribution of the nascent neutral product in terms of the transition dipole moment is proportional to $\cos^2 \chi$, in which χ is the angle between \vec{E} and \vec{M} [8]. In addition, the transition dipole moment matrix element \vec{M} contains the amplitude and phase information of the photoelectron partial waves that determine the MF photoelectron angular distributions (PAD) [9]. Therefore, the angular distributions of outgoing electrons, molecular axes of the parent anions and neutral products, and laser polarizations are in general all correlated.

The LF-PAD has been widely used to provide qualitative information such as the molecular symmetry and photodetachment dynamics for DPD

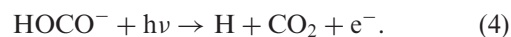
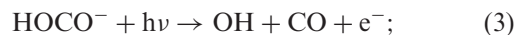
*Corresponding author. Email: rcontinetti@ucsd.edu

as well as other photodetachment processes [2,10,11]. However, significant information is lost due to the averaging over the randomly oriented parent anions. Noting that there exist two or more neutral dissociation fragments in a DPD process, one approach to the problem mentioned above is to record the PAD in coincidence with the angular distribution of the neutral photofragments. By this method, one can experimentally obtain the PAD in the photofragment recoil frame (RF), which in general contains more detailed dynamics information than the LF-PAD [12]. Specifically, if the dissociation occurs immediately following photoelectron ejection and the photofragments have an anisotropic angular distribution, the recoil angles of photofragments are directly related to the orientation of the breaking bonds at the moment of photoabsorption. In this case, measurement of the RF-PAD may help examine the interactions between the outgoing electron and the molecular core [4,5]. On the other hand, if the LF angular distribution of neutral photofragments is relatively isotropic, the RF-PAD will also tend to be isotropic and the analysis of both the RF-PAD and the LF photofragment angular distribution may yield important dynamics information such as the lifetime of the nascent neutral product and the orientation of the transition dipole in the molecular frame. Therefore, the measurement of the angular correlation between the photoelectrons and the neutrals as well as their angular distributions with respect to the laser polarization will reveal the DPD dynamics implied by Equation (1).

The current study focuses on the photoelectron-photofragment angular correlations in the DPD of a polyatomic anion, HOCO^- . With photoelectron-photofragment coincidence (PPC) spectroscopy, the DPD of HOCO^- has been used to explore the PES of $\text{OH} + \text{CO} \rightarrow [\text{HOCO}]^* \rightarrow \text{H} + \text{CO}_2$ [6,7], a fundamentally important reaction in hydrocarbon combustion that also regulates the OH, CO, and CO_2 concentrations in low atmosphere [13,14]. A number of previous studies have shown that along the minimum-energy $\text{OH} + \text{CO}$ reaction path, there exists a stable HOCO intermediate followed by a high reaction barrier before forming $\text{H} + \text{CO}_2$ [15–17], with an exoergicity relative to $\text{OH} + \text{CO}$ of -1.05 eV at 0 K [18]. In addition, two planar isomers, the *cis*- and *trans*-conformers were predicted for both the HOCO free radical and the HOCO^- anion [6,16–18]. Previous studies of the HOCO radical have been recently reviewed in detail in [7].

In this laboratory, the photodetachment of HOCO^- has been used to access the PES of the

HOCO radical at $E_{\text{hv}} = 4.80$ eV and 3.21 eV, with three neutral product channels observed [6,7]:



The measured channel-resolved photoelectron kinetic energy (eKE) spectra and PPC spectra reveal that the dominant photodetachment channel yields the stable HOCO free radical, consistent with the prediction of a deep HOCO potential well. At $E_{\text{hv}} = 3.21$ eV, PPC spectra and branching ratios for the DPD of HOCO^- and its deuterated form DOCO^- show evidence for a tunneling mechanism in the production of $\text{H} + \text{CO}_2$. Comparison of the PPC spectra with energetics and dynamics calculations indicated that DPD of vibrationally excited $\text{HOCO}^-/\text{DOCO}^-$ also contribute to the production of $\text{H}/\text{D} + \text{CO}_2 + e^-$, and is the major source of the $\text{OH}/\text{OD} + \text{CO} + e^-$ products [7,19].

With the adiabatic electron affinities (AEAs) of *cis*- and *trans*-HOCO predicted to be 1.43 eV and 1.30 eV respectively [6], the near-threshold photodetachment of HOCO^- was also carried out at $E_{\text{hv}} = 1.60$ eV to probe the bottom of the HOCO potential well [20]. In the photoelectron spectra two sharp peaks were resolved near threshold, and an additional broad peak around 1.2 eV was observed and assigned to a two-photon photodetachment process. The photoelectron kinetic energy (eKE)-dependent LF-PAD revealed that the one-photon photoelectron signal is composed of mixed *s*- and *p*-partial waves, while *p*-wave photodetachment becomes dominant at higher eKE. The two-photon photodetachment was shown to be accompanied by a unique four-fold LF-PAD, interpreted as the interfering *s*- and *d*-partial wave photoelectrons resulting from the photodetachment of an aligned temporary anion formed by a *p*-wave shape resonance near threshold. The relative amplitude and phase shift between *s*- and *d*-partial waves were obtained by a quantitative analysis of the two-photon LF-PAD, showing good agreement with the Wigner threshold law, as reported in [20].

This study presents further investigation of the DPD dynamics of HOCO^- and DOCO^- by examination of photoelectron and photofragment angular distributions and photoelectron-photofragment angular correlations. Following a brief description of the experimental methods, the RF-PAD of both the $\text{HOCO}^- + h\nu \rightarrow \text{OH} + \text{CO} + e^-$ and

$\text{HOCO}^- + h\nu \rightarrow \text{H} + \text{CO}_2 + e^-$ channels will be discussed. The LF neutral photofragment angular distribution of OH/OD + CO, from the one-photon photodetachment at $E_{\text{hv}} = 3.21 \text{ eV}$ and two-photon process at $E_{\text{hv}} = 1.60 \text{ eV}$ will then be presented. The RF-PAD will be compared with the corresponding LF-PAD. The relationship between the RF-PAD and the OH + CO recoil angles will also be examined. These results will be used to estimate the lifetime of the HOCO free radical and the orientation of transition dipole moment. Further evidence for the alignment of HOCO⁻ in the two-photon DPD process will also be presented.

2. Experiment

The experiments were carried out with a fast-ion-beam photoelectron-photofragment coincidence spectrometer which has previously been described in detail [3,6,7,20]. Therefore the experimental methods will only be briefly reviewed here. The HOCO⁻ was formed by crossing a 1 kHz pulsed supersonic expansion of a gas mixture (7% CO, 6% N₂O, 17% CH₄, and 70% N₂) with a 1 keV electron beam. In the DOCO⁻ experiment, CH₄ was replaced by CD₄ (99%, Cambridge Isotope Laboratory). The negative ions were then skimmed, accelerated to 10 keV, and referenced to ground potential by a high voltage switch. The HOCO⁻ with $m/e = 45$ ($m/e = 46$ for DOCO⁻) was mass selected by time-of-flight (TOF) and perpendicularly intercepted by a linearly polarized laser pulse. Two wavelengths, the fundamental (772 nm, $E_{\text{hv}} = 1.60 \text{ eV}$, $\sim 5 \times 10^{10} \text{ W/cm}^2$) and second harmonic (386 nm, $E_{\text{hv}} = 3.21 \text{ eV}$, $\sim 1 \times 10^{10} \text{ W/cm}^2$) from a Ti:Sapphire laser (Clark-MXR CPA-2000, 1.8 ps FWHM, 1 kHz) were used for the photodetachment measurements. The laser was linearly polarized, with \vec{E} fixed parallel to the ion beam propagation direction.

A space-focusing electron optics assembly was applied to collect the full 4π sr solid angle of photoelectrons [21]. The three-dimensional (3D) velocities of photoelectrons were measured by a time- and position-sensitive detector placed parallel to the plane of the laser and ion beams, allowing a straightforward detection of the PADs. The photoelectron detector was calibrated by the photodetachment of OH⁻ at 386 nm and O⁻ at 772 nm, with ΔE (full-width-at-half-maximum (FWHM)) = 0.18 and 0.06 eV at $eKE = 1.38$ and 0.14 eV, respectively. To remove the detector inhomogeneity in the LF-PAD, the data were symmetrized in the dimension along the ion beam propagation by an averaging procedure: $\tilde{N}(\theta_{\text{LF}}) = 1/2[N(\theta_{\text{LF}}) + N(180^\circ - \theta_{\text{LF}})]$. Here θ_{LF} is the

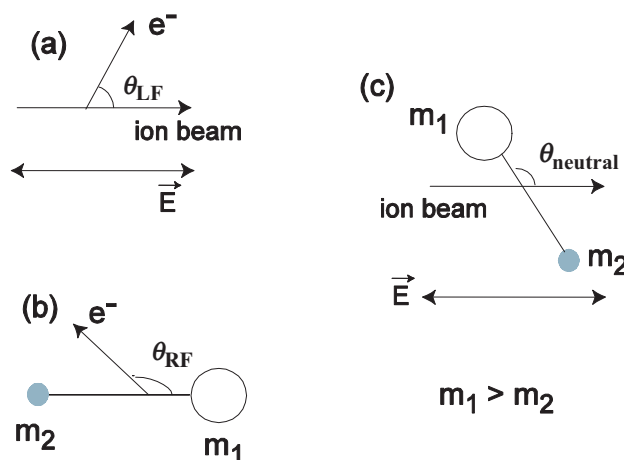


Figure 1. Angle definitions used in this work: (a) θ_{LF} , the laboratory frame (LF) photoelectron ejection angle with respect to the direction of ion beam propagation as well as the laser \vec{E} vector; (b) the recoil frame (RF) photoelectron ejection angle θ_{RF} with respect to the neutral photofragment recoil direction, $\theta_{\text{RF}} = 0^\circ$ when the photoelectron is ejected in the same direction as the heavier neutral fragment; (c) θ_{neutral} , the angle between the heavier neutral photofragment recoil and the direction of ion beam propagation.

laboratory frame angle between the photoelectron ejection and ion beam propagation directions (Figure 1(a)).

Undetached negative ions were deflected out of the ion beam by an electrostatic field and recorded by an ion detector. The neutral photofragments formed by photodetachment impinged on a time- and position-sensitive detector located 1.4 m away from the laser interaction region, perpendicular to the ion beam propagation. The masses and the 3D velocities in the centre of mass (CM) frame for the neutral products from a given DPD channel were determined by linear momentum conservation. The calibration of the photofragment detector was carried out by the DPD of O₄⁻ at 532 nm, showing a translational energy resolution of $\Delta E_T/E_T \sim 9\%$ at $E_T = 0.80 \text{ eV}$. The photoelectron and photofragments were recorded in an event-wise fashion in coincidence, making the measurement of the RF-PAD possible [4,5,22]. Similar to the LF-PAD, the detection inhomogeneity of the photoelectron detector was considered when analysing the RF-PAD. A two-dimensional data array was first generated, with one dimension θ_{RF} , the angle between the photoelectron and photofragment recoil directions (Figure 1(b)), and the other dimension θ_{LF} . The data were then symmetrized in the θ_{LF} dimension by $\tilde{N}(\theta_{\text{LF}}, \theta_{\text{RF}}) = 1/2[N(\theta_{\text{LF}}, \theta_{\text{RF}}) + N(180^\circ - \theta_{\text{LF}}, \theta_{\text{RF}})]$, followed by the summation of $\tilde{N}(\theta_{\text{LF}}, \theta_{\text{RF}})$ over θ_{LF} to generate a corrected $N(\theta_{\text{RF}})$ distribution. It has to be noted that

this treatment assumes full and homogeneous detection for photofragments that recoil forward and backward along the parent ion beam.

3. Results

In this section, the DPD dynamics of the HOCO and DOCO anions will be investigated by examination of both the LF photoelectron and photofragment angular distributions and the angular correlations of the photoelectron and photofragments in the recoil frame (RF). The photofragment angular distribution in the two-photon photodetachment of HOCO^- will also be presented.

Several different types of angles used in this work are defined in Figure 1. As mentioned in the experimental section, the LF photoelectron recoil angle θ_{LF} is chosen with respect to the direction of the ion beam and the collinear laser \vec{E} vector, with $\theta_{LF}=0$ when the electron is ejected along the fast ion beam towards the photofragment detector (Figure 1(a)). The RF photoelectron recoil angle θ_{RF} is defined to be zero when the electron is ejected in the same direction as that of the larger mass of the two neutral dissociation products (CO for OH + CO and CO_2 for the H + CO_2 channel) (Figure 1(b)). Similarly, the LF neutral photofragment recoil angle $\theta_{neutral}=0$ when the heavier photofragment recoils along the direction of ion beam propagation (Figure 1(c)).

3.1. LF- and RF-PAD in one-photon DPD

The LF-PAD in one photon photodetachment of isotropically distributed anions can be described by the differential cross section [23]:

$$\frac{d\sigma}{d\theta_{LF}} = \frac{\sigma_{tot}}{4\pi} [1 + \beta_2 P_2(\cos \theta_{LF})], \quad (5)$$

where σ_{tot} is total cross-section integrated over the full 4π sr solid angle, β_2 is the energy-dependent anisotropy parameter, and $P_2(\cos \theta_{LF})$ is the second-order Legendre polynomial in $\cos \theta_{LF}$. The β_2 value in Equation (5) is limited between -1 and 2 . Photoejection of a p -wave photoelectron leads to $\beta_2 = 2$, resulting in $(d\sigma/d\theta_{LF}) \propto \cos^2 \theta_{LF}$; when $\beta_2 = 0$, an isotropic LF-PAD is expected, consistent with s -wave photodetachment; when $\beta_2 = -1$, $(d\sigma/d\theta_{LF})$ is proportional to $\sin^2 \theta_{LF}$ as a result of interfering s - and d -photoelectron partial waves [23].

Compared with the LF-PAD, the MF-PAD can provide richer information about the photodetachment

dynamics since it describes the molecular-geometry-dependent electron scattering process [24]:

$$\frac{d^2\sigma}{d\theta d\phi} = \sum_{L=0}^{L_{\max}} \sum_{M=-L}^L B_{L,M} Y_{L,M}(\theta, \phi), \quad (6)$$

where $B_{L,M}$ is the coefficient containing the radial dipole matrix element and the relative phase of the photoelectron partial wave, and $Y_{L,M}(\theta, \phi)$ are the appropriate spherical harmonics. However, the MF-PAD can only be determined from molecules fixed-in-space. In a DPD experiment on a polyatomic molecule, the only available reference axis is the recoil frame (RF) defined by the neutral photofragment recoil direction. As a result, the ϕ term in Equation (6) is not observable and the differential cross section for the RF-PAD can be described by [22]:

$$\frac{d\sigma}{d\theta_{RF}} = \frac{\sigma_{tot}}{4\pi} \left[1 + \sum_{i=1}^{i_{\max}} A_i P_i(\cos \theta_{RF}) \right], \quad (7)$$

in which A_i and P_i represent the i th-order anisotropy parameter and Legendre polynomials, respectively. Specifically, the A_i values with the odd i will determine the forward-backward asymmetry in the RF-PAD if there is any [22].

Equations (5) and (7) are used to interpret the LF- and RF-PADs obtained from one-photon photodetachment of HOCO^- and DOCO^- ($E_{\text{hv}} = 3.21$ eV) presented in Figure 2. The PADs in the two frames are plotted in the form of $N(\cos \theta_{LF})$ versus $\cos \theta_{LF}$ and $N(\cos \theta_{RF})$ versus $\cos \theta_{RF}$, respectively, to avoid the zero distributions at 0° and 180° caused by the $\sin \theta$ term when integrating over the solid angle. The $N(\cos \theta)$ represents the number of events within a histogram between $\cos \theta$ and $\cos \theta + \Delta(\cos \theta)$ and is integrated over the whole eKE distribution. In Figure 2, the number of bins is chosen to be 32 for each histogram.

Using Equation (5), the one-photon LF-PADs at $E_{\text{hv}} = 3.21$ eV in Figure 2(a)–(d) are fitted, yielding the LF photoelectron anisotropy parameter $\beta_2 = 1.1, 1.4, 1.0$ and 1.3 ± 0.1 for the DPD channels OH + CO + e^- , H + CO_2 + e^- (from the DPD of HOCO^-), OD + CO + e^- , and D + CO_2 + e^- (from the DPD of DOCO^-), respectively. The observation that $\beta_2 \geq 1.0$ for all four of the DPD channels is consistent with a dominant p -wave photodetachment process, causing the LF-PAD to peak parallel to the laser polarization [23]. The LF-PAD in the H/D + CO_2 + e^- channel is seen to be more anisotropic than that in the OH/OD + CO_2 + e^- channel. As the H/D + CO_2 + e^- channel corresponds to a higher

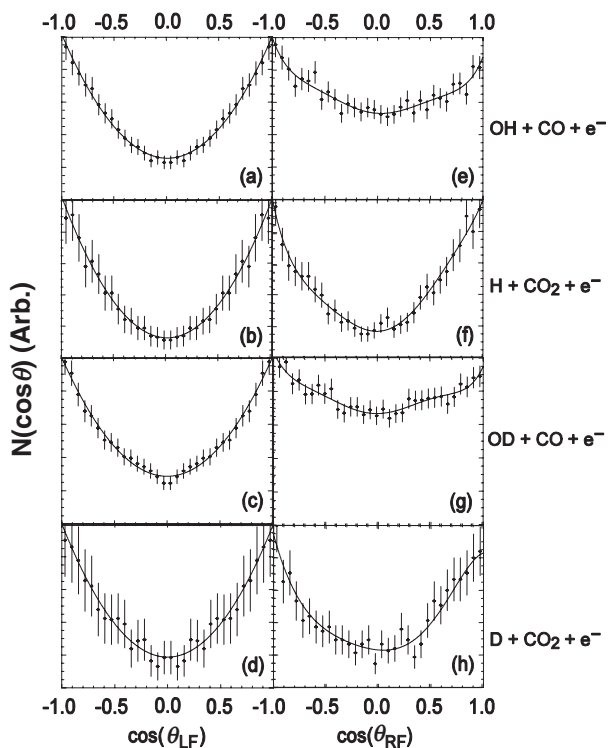


Figure 2. The LF- (left column) and RF-PADs (right column) of $\text{OH} + \text{CO} + e^-$ (top row), $\text{H} + \text{CO}_2 + e^-$ (the second row from the top), $\text{OD} + \text{CO} + e^-$ (the third row from the top), and $\text{D} + \text{CO}_2 + e^-$ (bottom row) from the one-photon photodetachment of HOCO^- and DOCO^- at $E_{\text{hv}} = 3.21$ eV. The scattered dots represent the number of events recorded within a small range of $\cos\theta$, with $\pm 1\sigma$ Poisson error bars. The solid lines are from fitting the experimental data using Equation (5) for LF- and Equation (7) for RF-PADs.

eKE distribution, the observed larger β_2 value in the $\text{H/D} + \text{CO}_2 + e^-$ channel implies a more dominant p -partial wave at higher eKE, consistent with our previous results and the prediction of the Wigner threshold law that the larger l -partial waves are suppressed near the photodetachment threshold, becoming more dominant as eKE increases [20,25,26]. As seen from the measured β_2 values, the isotopic effect on the LF-PAD's is negligible with the current uncertainties, implying that the photoelectron experiences similar interactions during escape from the HOCO and DOCO neutral cores.

The channel-resolved RF-PADs produced by the one-photon photodetachment of HOCO^- and DOCO^- are presented in Figure 2(e)–(h). Equation (7) was used to fit the observed RF-PADs, with $i_{\text{max}} = 6$. The resulting RF photoelectron anisotropy parameters A_i are listed in Table 1. It is seen that $A_2 = 0.4 \pm 0.1$ for $\text{OH} + \text{CO} + e^-$ and 0.3 ± 0.1 for $\text{OD} + \text{CO} + e^-$ channel, while the other A_i values are all equal or close to zero, showing that the RF-PADs in this DPD channel are more isotropic compared with the corresponding LF-PADs ($\beta_2 = 1.1$ for $\text{OH} + \text{CO} + e^-$ and 1.0 for $\text{OD} + \text{CO} + e^-$). On the other hand, the RF-PADs in the hydrogen production channel show more significant anisotropies, with $A_2 = 1.4 \pm 0.1$ and 1.1 ± 0.1 for $\text{H} + \text{CO}_2 + e^-$ and $\text{D} + \text{CO}_2 + e^-$ channels, respectively. These two A_2 values are very close to the LF photoelectron β_2 . A set of other non-zero A_i parameters are also obtained in $\text{H/D} + \text{CO}_2 + e^-$ channel as seen in Table 1.

Table 1. Anisotropy parameters for the RF-PADs from one- and two-photon DPD of HOCO^- and DOCO^- . For $\text{OH}/\text{OD} + \text{CO} + e^-$, the RF-PAD anisotropy parameters are also reported as a function of the neutral photofragment recoil angles relative to the laser electric vector. The uncertainties for A_i are estimated to be ± 0.1 for one-photon measurements and ± 0.2 for two-photon measurements.

	θ_{neutral}	A_1	A_2	A_3	A_4	A_5	A_6
One-photon, $E_{\text{hv}} = 3.21$ eV							
$\text{OH} + \text{CO} + e^-$	$[0^\circ, 180^\circ]$	-0.1	0.4	0.0	0.0	0.0	0.1
	$[0^\circ, 18^\circ]$ & $[162^\circ, 180^\circ]$	0.1	1.0	0.0	-0.1	-0.1	0.0
	$[18^\circ, 60^\circ]$ & $[120^\circ, 162^\circ]$	-0.1	0.4	0.0	0.10	0.0	0.1
	$[60^\circ, 120^\circ]$	-0.1	-0.2	0.0	0.0	0.0	0.1
$\text{OD} + \text{CO} + e^-$	$[0^\circ, 180^\circ]$	0.0	0.3	0.0	0.0	0.0	0.1
	$[0^\circ, 25^\circ]$ & $[155^\circ, 180^\circ]$	0.0	0.7	0.1	0.1	0.1	0.1
	$[25^\circ, 60^\circ]$ & $[120^\circ, 155^\circ]$	0.0	0.3	0.0	0.0	0.0	0.1
	$[60^\circ, 120^\circ]$	0.0	-0.3	0.0	0.0	0.1	0.0
$\text{H} + \text{CO}_2 + e^-$	All detected	0.3	1.4	0.2	0.2	0.2	0.2
$\text{D} + \text{CO}_2 + e^-$	All detected	0.2	1.1	-0.1	0.1	-0.1	0.1
Two-photon, $E_{\text{hv}} = 1.60$ eV							
$\text{OH} + \text{CO} + e^-$	$[0^\circ, 180^\circ]$	0.1	-0.1	0.0	0.4	0.0	0.0
$\text{H} + \text{CO}_2 + e^-$	All detected	0.5	0.2	0.3	1.4	0.1	0.1

3.2. LF photofragment angular distributions

Because the neutral photofragment recoil axis is used as the reference in generation of the RF-PAD, to further understand the RF-PADs shown in Figure 2, the LF photofragment angular distributions obtained from the one-photon DPD of $\text{HOCO}^-/\text{DOCO}^-$ at $E_{\text{hv}} = 3.21$ eV must also be examined. Figure 3(a) and (b) show the OH/OD + CO LF angular distribution in the form of $N(\theta_{\text{neutral}})$ versus θ_{neutral} , in which $N(\theta_{\text{neutral}})$ is defined as the number of events within a small range of recoil angles from θ_{neutral} to $\theta_{\text{neutral}} + \Delta\theta_{\text{neutral}}$ and $\Delta\theta_{\text{neutral}}$ is set to 4° . These distributions have not been symmetrized in any way, showing that the assumption used in symmetrization of the RF-PADs is a good one. The $N(\theta_{\text{neutral}})$ distributions instead of $N(\cos\theta_{\text{neutral}})$ were plotted because not all the photofragments can be detected as discussed below.

The differential cross-section defined by Equation (5) is also valid for the characterization of the photofragment angular distribution in LF when θ_{LF} is replaced by θ_{neutral} [27]. However, the detection of neutral photofragments is more complicated than that of the photoelectrons. For example, the measurement of the two neutral dissociation products in coincidence involves consideration of the detector acceptance function (DAF), and the detector efficiency may vary with different masses. In addition, detection of the two dissociation products is affected by the 19 ns dead time of the detector. Consequently, the experimental $N(\theta_{\text{neutral}})$ curves in Figure 3(a) and (b) cannot be simply fitted by Equation (5). To faithfully model the DAF and obtain a reliable photofragment anisotropy parameter β_2 , a Monte Carlo simulation incorporating Equation (5) was employed in the current study to reproduce the observed $N(\theta_{\text{neutral}})$ distributions [28,29]. In Figure 3, the solid and dashed lines represent the experimental and simulated $N(\theta_{\text{neutral}})$, respectively. The β_2 values of 0.8 ± 0.1 for OH + CO and 0.6 ± 0.1 for OD + CO are obtained, showing that the OH + CO products also recoil along the laser \vec{E} vector but are more isotropic than the LF-PADs for those channels.

The observed H/D + CO₂ LF photofragment angular distributions also peak along the laser \vec{E} vector and are much more anisotropic than that of the OH/OD + CO, but this is to first order a result of the very limited DAF for H/D atom detection. The kinetic energy release (KER) was found to peak around 0.5 eV for the H/D + CO₂ products at $E_{\text{hv}} = 3.21$ eV [7]. Due to the large mass difference between H/D atoms and CO₂ and linear momentum conservation, only the H atoms with $\theta_{\text{neutral}} \leq \sim 17^\circ$ or $\theta_{\text{neutral}} \geq \sim 161^\circ$ and the D atoms

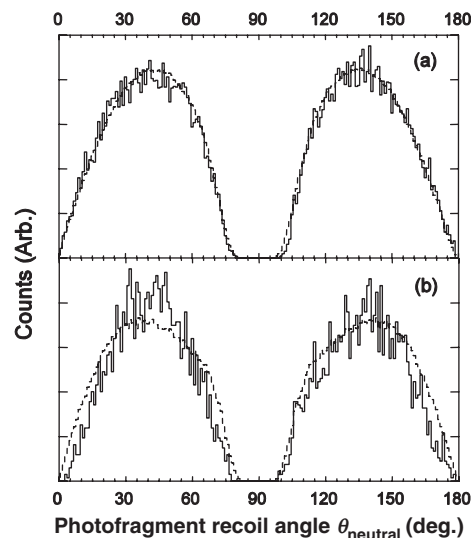


Figure 3. The LF photofragment angular distributions for (a) OH + CO and (b) OD + CO from the one-photon photodetachment of HOCO^- and DOCO^- at $E_{\text{hv}} = 3.21$ eV. Solid lines are experimental results. Dashed lines were obtained by the Monte Carlo simulation using Equation (5).

with $\theta_{\text{neutral}} \leq \sim 25^\circ$ or $\theta_{\text{neutral}} \geq \sim 154^\circ$ can be detected, while the majority of H/D atoms recoil out of the ion beam and miss the photofragment detector. The Monte Carlo simulation coupled with Equation (5) was carried out for the H/D + CO₂ products. However, the simulated angular distribution is insensitive to β_2 values ranging from -1 to 2 . Therefore, the Monte Carlo simulations for H/D + CO₂ did not yield meaningful photofragment β_2 values.

The general trends observed in the RF-PADs in Figure 2 can be explained by the photofragment angular distributions discussed above. The RF-PAD's in the OH/OD + CO + e⁻ channel are more isotropic than the corresponding LF-PAD because the OH + CO products recoil at a relatively wide range of angles with respect to the laser \vec{E} vector, as a result of rotation during the lifetime of the HOCO/DOCO intermediate and the angle between the transition dipole and breaking HO-CO bond. The more anisotropic RF-PAD's in H/D + CO₂ + e⁻ channel, however, are likely to result from the small DAF for detection of the H/D + CO₂ products.

To verify this assertion, the RF-PAD of the OH/OD + CO + e⁻ channel with the OH/OD + CO recoil axis restricted in a range of solid angles to the laser polarization was examined, as demonstrated in Figure 4. The figure shows that when the OH/OD + CO recoil axis is restricted around the laser \vec{E} vector [$0^\circ \leq \theta_{\text{neutral}} \leq 18^\circ$ or $162^\circ \leq \theta_{\text{neutral}} \leq 180^\circ$ for OH + CO in Figure 4(a), and $0^\circ \leq \theta_{\text{neutral}} \leq 25^\circ$ or

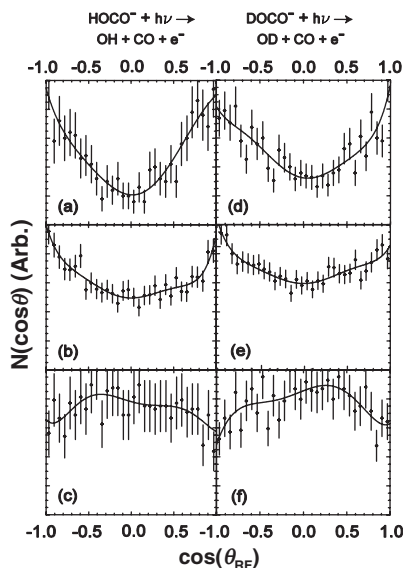


Figure 4. RF-PADs in the one-photon DPD channels $\text{HOCO}^- + h\nu \rightarrow \text{OH} + \text{CO} + e^-$ (left column) and $\text{DOCO}^- + h\nu \rightarrow \text{OD} + \text{CO} + e^-$ (right column) at $E_{h\nu} = 3.21 \text{ eV}$ with the neutral photofragment recoil angles restricted within (a) $0^\circ \leq \theta_{\text{neutral}} \leq 18^\circ$ or $162^\circ \leq \theta_{\text{neutral}} \leq 180^\circ$; (b) $18^\circ \leq \theta_{\text{neutral}} \leq 60^\circ$ or $120^\circ \leq \theta_{\text{neutral}} \leq 162^\circ$; (d) $0^\circ \leq \theta_{\text{neutral}} \leq 25^\circ$ or $155^\circ \leq \theta_{\text{neutral}} \leq 180^\circ$; (e) $25^\circ \leq \theta_{\text{neutral}} \leq 60^\circ$ or $120^\circ \leq \theta_{\text{neutral}} \leq 155^\circ$; and (c) and (f) $60^\circ \leq \theta_{\text{neutral}} \leq 120^\circ$. The scattered dots represent experimental intensity with $\pm 1\sigma$ Poisson error bars. The solid lines are from fitting the experimental data using Equation (5) for LF- and Equation (7) for RF-PADs.

$155^\circ \leq \theta_{\text{neutral}} \leq 180^\circ$ for $\text{OD} + \text{CO}$ in Figure 4(e)], a more anisotropic RF-PAD is observed to peak parallel to the $\text{OH}/\text{OD} + \text{CO}$ recoil axis. Here the θ_{neutral} range is chosen to be consistent with the maximum photofragment recoil angle of 18° for $\text{H} + \text{CO}_2$ and 25° for $\text{D} + \text{CO}_2$ so that the RF-PADs in Figure 4(a) and (e) can be compared with those in Figure 2(f) and (h). Within this θ_{neutral} range, $A_2 = 1.0 \pm 0.1$ for $\text{OH} + \text{CO} + e^-$, consistent with the LF photoelectron $\beta_2 = 1.1 \pm 0.1$; while $A_2 = 0.7 \pm 0.1$ for $\text{OD} + \text{CO} + e^-$, smaller than the corresponding LF photoelectron $\beta_2 = 1.0 \pm 0.1$ and consistent with a longer lifetime for DOCO and a relatively wider angular range for photofragment recoil [$0-25^\circ$ compared with $0-18^\circ$ chosen for $\text{OH} + \text{CO}$ in Figure 4(a)]. When the $\text{OH}/\text{OD} + \text{CO}$ recoil axis is limited to be perpendicular to the laser electric field [$60^\circ \leq \theta_{\text{neutral}} \leq 120^\circ$, as in Figure 4(c) and (g)], A_2 becomes slightly negative and the RF-PAD's are more isotropic. Limiting the $\text{OH}/\text{OD} + \text{CO}$ recoil axis in a range between these two extremes [$18^\circ \leq \theta_{\text{neutral}} \leq 60^\circ$ or $120^\circ \leq \theta_{\text{neutral}} \leq 162^\circ$ for $\text{OH} + \text{CO}$ in Figure 4(b), and $25^\circ \leq \theta_{\text{neutral}} \leq 60^\circ$ or $120^\circ \leq \theta_{\text{neutral}} \leq 155^\circ$ for $\text{OD} + \text{CO}$ in Figure 4(f)], the observed RF-PADs are very similar to those without

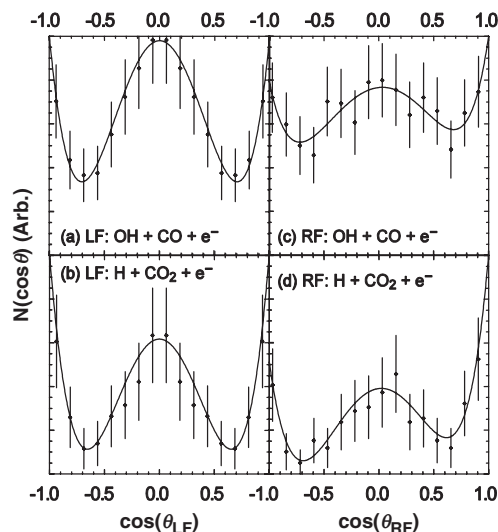


Figure 5. The LF (left column) and RF-PADs (right column) of (a) and (c) $\text{HOCO}^- + h\nu \rightarrow \text{OH} + \text{CO} + e^-$, and (b) and (d) $\text{HOCO}^- + h\nu \rightarrow \text{H} + \text{CO}_2 + e^-$ at $E_{h\nu} = 1.60 \text{ eV}$. The scattered dots represent experimental intensity, with $\pm 1\sigma$ Poisson error bars. The solid lines are from fitting the experimental data using Equation (8) for LF- and Equation (7) for RF-PADs.

the limitation of $\text{OH}/\text{OD} + \text{CO}$ recoil axis shown in Figure 2(e) and (g). The anisotropy parameters obtained by fitting each of the RF-PADs in Figure 4 are included in Table 1, showing the significant dependence of RF-PAD on the photofragment recoil direction for $\text{OH} + \text{CO} + e^-$, consistent with the anisotropic RF-PAD seen in $\text{H} + \text{CO}_2 + e^-$.

3.3. Angular correlations in two-photon DPD

The photoelectron-photofragment correlations have also been investigated for two-photon photodetachment of HOCO^- at $E_{h\nu} = 1.60 \text{ eV}$. Our previous study has shown the co-existence of parallel and perpendicular LF-PADs in this two-photon process, interpreted to result from interfering s - and d -photoelectron partial waves mediated by a near-threshold p -type shape resonance [20]. Figure 5 compares the channel-resolved LF- and RF-PADs from the two-photon DPD processes. Equation (5) used for the LF-PAD in one-photon photodetachment is not suitable for a two-photon process, a fourth-order Legendre polynomial and its corresponding anisotropy parameter must be included in the differential cross-section [30]:

$$\frac{d\sigma}{d\theta_{LF}} = \frac{\sigma_{\text{tot}}}{4\pi} [1 + \beta_2 P_2(\cos\theta_{LF}) + \beta_4 P_4(\cos\theta_{LF})]. \quad (8)$$

Using Equation (8), the LF photoelectron anisotropy parameters $\beta_2 = -0.4 \pm 0.2$ and $\beta_4 = 0.9 \pm 0.2$ were obtained for the $\text{OH} + \text{CO} + e^-$ channel integrated over all eKE, indicating that the perpendicular component is more dominant. On the contrary, in the $\text{H} + \text{CO}_2 + e^-$ channel, $\beta_2 = 0.0 \pm 0.2$ and $\beta_4 = 1.6 \pm 0.2$, corresponding to a more parallel component. The observed difference in the LF-PAD of these two DPD channels can simply be explained by the eKE-dependence of *s*- and *d*-photoelectron partial wave interference. The $\text{OH} + \text{CO} + e^-$ channel yields a lower-eKE distribution than the $\text{H} + \text{CO}_2 + e^-$ channel, and therefore corresponds to a more dominant *s*-wave component in the interference and consequently a more perpendicular feature in the LF-PAD [20].

The RF anisotropy parameter A_i values were also obtained for these two DPD processes and listed in Table 1. Similar to the one-photon measurement, the RF-PAD in the $\text{OH} + \text{CO} + e^-$ channel is more isotropic than the corresponding LF-PAD as $A_2 = -0.1 \pm 0.2$ and $A_4 = 0.4 \pm 0.2$, consistent with a relatively isotropic angular distribution for the photoelectron relative to the $\text{OH} + \text{CO}$ recoil directions; while the RF-PAD for $\text{H} + \text{CO}_2 + e^-$ shows a significant anisotropy with $A_2 = 0.2 \pm 0.2$ and $A_4 = 1.4 \pm 0.2$, in agreement with the small solid angle of $\text{H} + \text{CO}_2$ products being detected.

The photofragment angular distributions for $\text{OH} + \text{CO}$ products were also measured to directly evaluate the alignment of the HOCO^- anions via a shape resonance reported in [20]. Figure 6 shows the $N(\theta_{\text{neutral}})$ versus θ_{neutral} in the LF for $\text{OH} + \text{CO}$ obtained from the two-photon DPD of HOCO^- at $E_{\text{hv}} = 1.60 \text{ eV}$. A Monte Carlo simulation using Equation (8) was used to fit the experimental data, showing the LF anisotropy parameters $\beta_2 = 1.3 \pm 0.2$ and $\beta_4 = 0.3 \pm 0.2$. Further discussion about the photofragment angular distribution in the two-photon DPD of HOCO^- will be presented in the next section.

4. Discussion

The photoelectron-photofragment angular correlations can provide deep insights into the dynamics of a DPD process, particularly in the case of ultrafast dissociation of the molecular framework. In the case of the DPD of HOCO^- onto the ground state potential energy surface of HOCO , however, dissociation of the HOCO radical is not instantaneous, and thus the RF-PADs representing the best direct measure of MF-PAD are blurred significantly by a separation of

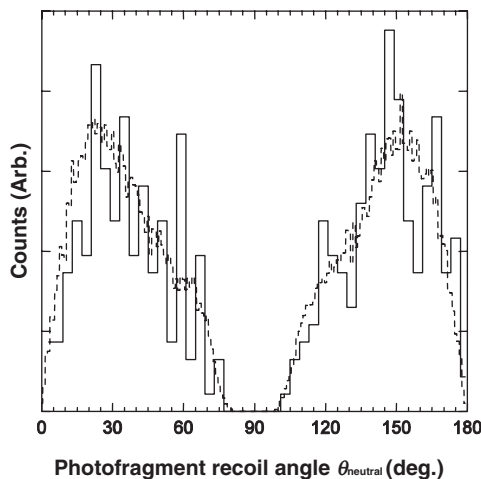


Figure 6. The LF photofragment angular distributions of $\text{OH} + \text{CO}$ from the two-photon photodetachment of HOCO^- at $E_{\text{hv}} = 1.60 \text{ eV}$. Solid lines are from experimental measurements. Dashed lines represent the Monte Carlo simulation results using Equation (8).

time scales for photodetachment and subsequent dissociation of the molecular frame. Thus, in the present work we will focus primarily on assessing the implications of the LF-PAD and LF photofragment angular distributions on the radical lifetime and the symmetry and orientation of the transition dipole in the molecular frame. The $\text{OH} + \text{CO}$ angular distributions from the two-photon DPD of HOCO^- will also be discussed, providing further evidence for the alignment of HOCO^- in a near-threshold shape resonance.

4.1. LF-PAD in one-photon DPD of $\text{HOCO}^- | \text{DOCO}^-$

A theoretical prediction of the observed LF-PAD requires a high-level electron-molecule scattering calculation, beyond the scope of the present study. An approximate group-theoretical treatment, limiting the continuum electron states to *s*- & *p*-waves, as presented by Sanov and coworkers is employed here to explain the observed LF-PAD qualitatively [10].

From a symmetry perspective, a dipole-allowed photodetachment process requires the direct product of irreducible representations for the transition dipole moment and wave functions of the initial anion and final products (electron+neutral) to contain the completely symmetric irreducible representation. Previous high level *ab initio* calculations showed that both HOCO^- and the ground electronic state of the HOCO free radical have A' symmetry in C_s geometry [6,31]. The direct product of the initial and final state

symmetries and the transition dipole can then be described by $A'(\text{anion}) \otimes a'(\mu_{x,y}) \otimes A'(\text{radical}) \otimes \varphi_{ele}$ for the x and y components (in the plane of symmetry), and $A'(\text{anion}) \otimes a''(\mu_z) \otimes A'(\text{radical}) \otimes \varphi_{ele}$ for the z component (perpendicular to the plane of symmetry). These two direct products must contain the completely symmetric A' representation in the C_s point group. With the assumption that only s - and p -wave photodetachment is involved, it is predicted that the photoelectron wave function is isotropic (s -type photoelectron) or parallel to the HOCO plane (p_x, p_y -type) for a dipole transition in the symmetry plane, and perpendicular to the HOCO plane (p_z -type) for a dipole transition perpendicular to the symmetry plane. In the electric-dipole approximation, the transition dipole tends to lie along the laser electric field. As a result, the one-photon LF-PAD's for p -wave photodetachment with both parallel and perpendicular transitions are predicted to be parallel to the laser polarization. To determine whether the dipole transition in the DPD of HOCO^- is parallel or perpendicular to the symmetry plane, the LF angular distributions of neutral photofragments also have to be inspected.

4.2. LF photofragment angular distribution in one-photon DPD of $\text{HOCO}^-/\text{DOCO}^-$

As shown in the results section, the OH/OD + CO photofragments have positive anisotropy parameters, consistent with recoil of the OH/OD + CO products along the laser polarization and thus a dipole transition in the HOCO plane. For more detailed investigation of the dynamical information conveyed by the observed LF angular distributions of the neutral photofragments, a classical model developed by Busch and Wilson is used [8]. This model treats a polyatomic molecule as a pseudodiatom case. Assuming the chemical bond breaks at a given angle γ to the transition dipole \vec{M} and taking the tangential velocity v_t resulting from rotation of the parent molecule and the lifetime τ of the photoexcited state into account, the photofragment anisotropy parameter β_2 can be calculated using the equation (8)

$$\frac{\beta_2}{2} = \left\{ [P_2(\alpha) + \eta^2 - 3\eta \sin \alpha \cos \alpha] / 1 + 4\eta^2 \right\} P_2(\cos \gamma) \quad (9)$$

Here, $\alpha = \sin^{-1}(v_t/v)$ where v is the photofragment recoil velocity, v_t is the tangential velocity component due to parent rotation, and $\eta = \omega\tau$ where ω is the angular velocity of rotation of the photoexcited state. The definitions of the angles involved in Equation (9) are shown in Figure 7.

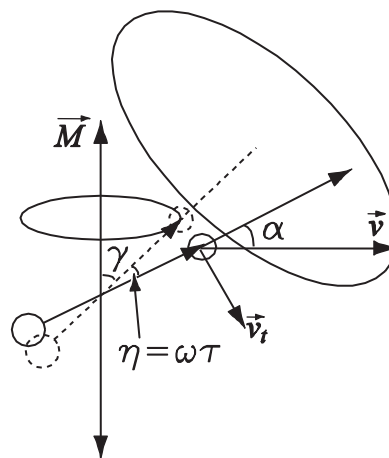


Figure 7. Schematic pseudodiatom model of Busch and Wilson [8]. The included angle between the breaking bond and the transition dipole is γ . The excited molecule rotates an angle of $\eta = \omega\tau$ in the lifetime of τ . An additional deflection of the photofragment recoil direction by an angle of α is caused by the rotation in the initial state, and can be calculated by $\alpha = \sin^{-1}(v_t/v)$ where v is the photofragment recoil velocity and v_t is the tangential velocity in rotation of the initial state.

Although first developed for photodissociation processes, Equation (9) is also valid for the interpretation of photofragment angular distributions involved in a DPD process since the angular momentum of the photoelectron is negligible. In Equation (9), the β_2 parameters for OH/OD + CO have been experimentally measured. It is noted that the peak kinetic energy release (KER) of OH/CO + CO products is ≈ 0.1 eV, giving an estimated v value of 8.4×10^4 cm/s for OH and 8.1×10^4 cm/s for OD [7]. The estimation of v_t makes use of the equilibrium geometry from *ab initio* calculations [6,32]. The moments of inertia of the CM of the OH/OD group in $\text{HOCO}^-/\text{DOCO}^-$ and the total moments of inertia of the anion (Table 2) were calculated respectively for both the *trans*- and *cis*-configurations, since the *cis*- and *trans*- isomers are indistinguishable in the parent ion beam. The fractions of the rotational energy of the CM of OH/OD over the total rotational energy of $\text{HOCO}^-/\text{DOCO}^-$ then can be estimated for all three principal axes, while the total rotational energy of the anion is taken to be $1/2kT$ for each principal axis based on the equipartition principle. A typical rotational temperature of $T = 35$ K in the supersonic expansion was used here because the rotational relaxation is expected to be efficient in the ion source, although vibrationally excited $\text{HOCO}^-/\text{DOCO}^-$ anions exist in the parent ion beam as discussed previously [7]. The values of v_t for the OH/OD fragments were then calculated from $E_{\text{rot}} = 1/2m v_t^2$, where E_{rot} is the sum of rotational

Table 2. Moments of inertia for HOCO/DOCO (in atomic units $\text{amu}\cdot\text{a}_0^2$) calculated using the equilibrium geometry from *ab initio* calculations [6,32].

	I_A	I_B	I_c
<i>trans</i> -HOCO ⁻	21	164	186
<i>cis</i> -HOCO ⁻	24	146	169
<i>trans</i> -DOCO ⁻	22	175	197
<i>cis</i> -DOCO ⁻	27	148	176
<i>trans</i> -HOCO	11	160	171
<i>cis</i> -HOCO	13	156	169
<i>trans</i> -DOCO	12	171	184
<i>cis</i> -DOCO	17	160	177

energies of the CM of the OH/OD products about the three principal axes. Since the calculations presented here are only the approximations and the obtained α values are very similar, an averaged $\alpha(\text{OH/OD})=9.3^\circ$ was used. This relatively large value for α is a measure of the breakdown of the axial recoil approximation for the small KER and relatively heavy OH/OD fragments involved in this channel.

With the measured photofragment β_2 parameter and α angle, Equation (9) can be used to calculate the relationship between the orientation of the transition dipole with respect to the breaking HO-CO (DO-CO) bond and the HOCO/DOCO lifetime prior to dissociation into OH/OD + CO. The functions of η versus γ for OH + CO (solid line) and OD + CO (dashed line) are plotted in Figure 8, showing that if the HO-CO or DO-CO bond breaks in a direction parallel to the transition dipole ($\gamma=0^\circ$), the HOCO and DOCO rotate ~ 0.7 and ~ 1.0 radians, respectively, before dissociating into OH/OD + CO fragments. On the other hand, if the HOCO and DOCO radicals have negligible rotation before dissociation, the transition dipole is oriented at a maximum angle of $\sim 38^\circ$ to the HO-CO bond and $\sim 42^\circ$ to the DO-CO bond. Based on the fact that $\gamma \leq \sim 38^\circ$, a perpendicular transition can be quantitatively excluded since it requires $\gamma=90^\circ$. In addition, the transition dipole can be predicted to lie within $\pm 38^\circ$ from the HO-CO bond within the HOCO plane.

Although the exact lifetime of the HOCO and DOCO radicals before dissociation into OH/OD + CO products cannot be obtained due to the uncertain γ angle, an upper limit for the lifetime for HOCO/DOCO from $\tau = \eta/\omega$ can be estimated. An estimate for ω is once again based on the equipartition principal, $E_{\text{rot}} = 1/2 I \omega^2 = 1/2 kT$ for each principal axis. The moments of inertia of HOCO/DOCO radicals are listed in Table 2. Since an upper limit for the lifetime is desired, among the three ω values, the smallest one about the major principal

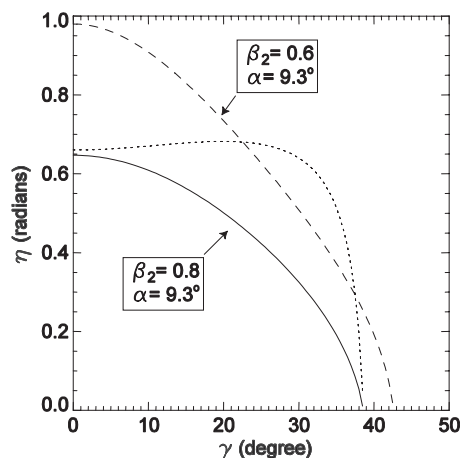


Figure 8. Rotation angle $\eta = \omega\tau$ as a function of γ , the angle between the breaking bond and transition dipole for OH + CO (solid line) and OD + CO (dashed line). The dotted line shows the ratio of $\eta(\text{OH} + \text{CO})/\eta(\text{OD} + \text{CO})$ as a function of γ , and can also be read from the y-axis ranging from 0 to 1 as a dimensionless quantity.

axis perpendicular to the HOCO/DOCO plane (corresponding to the largest moment of inertia), is used in this calculation. From Figure 8, $\eta \leq 0.7$ radians for OH + CO and 1.0 radian for OD + CO, therefore, the upper limits to the lifetime, $\tau \leq 9 \times 10^{-13}$ s and 1.3×10^{-12} s, are obtained for the HOCO and DOCO free radicals leading to OH/OD + CO formation. These upper limits are consistent with the previously reported HOCO lifetime from a femtosecond pump-probe measurement of OH products in the photoinduced reaction of $\text{CO}_2\text{-HI}$ van der Waals complexes carried out by Wittig and co-workers although these authors estimated 50% uncertainties for their measurement [33], but smaller than that obtained from a similar picosecond experiment conducted by Zewail and co-workers [34].

Deuterium substitution in the HOCO radical only affects the zero point energy and vibrational and rotational energy spacing, and has no influence on the PES shape. Thus it is reasonable to assume that, on average, the OH + CO and OD + CO products have the same γ angle. The dotted line in Figure 8 represents the function of $\eta(\text{OH} + \text{CO})/\eta(\text{OD} + \text{CO})$ versus γ , indicating that HOCO has a lifetime of around 60–70% of that of DOCO for γ angles ranging up to $\sim 30^\circ$. Noting that the difference of the HOCO and DOCO lifetimes originates from the β_2 parameters that differ by 0.2, this lifetime difference is likely to be smaller than that shown in Figure 8 owing to the uncertainty of ± 0.1 for each β_2 . Nevertheless, the observed deuterium effect in the lifetime may be related to the previously reported sensitivity of HOCO

lifetime to different rotational or spin-orbit states in OH [$(^2\Pi_{1/2}, N)$ and $(^2\Pi_{3/2}, N)$] products [33–35]. Because the moment of inertia for OD is nearly the double of that for OH, the OD products in a DPD process can be more rotationally excited than OH. Therefore, the observed lifetime difference for HOCO and DOCO may correlate to the different rotational distributions in OH and OD products [33,35]. State-selective detection of the OH products, by laser induced fluorescence for example, coupled with the DPD experiment, would be helpful to answer this question but exceedingly difficult.

It has to be noted that the lifetime discussion here is only an estimate. Besides all the approximations mentioned above, HOCO is a polyatomic molecule that is vibrating during the dissociation. Consequently, the HO–CO bond can break at a distribution of γ angles simply as a result of molecular vibration and zero-point motion, making Equation (9) less suitable for the calculation of lifetime. In addition, the production of OH/OD + CO primarily results from photodetachment of vibrationally excited HOCO[−]/DOCO[−] as discussed in the previous study [7]. Therefore, consideration of rotational effects in the parent anion needs to be extended to excited vibrational states as well, beyond the scope of the current study.

In the case of the one-photon DPD channel of H/D + CO₂ + e[−] at $E_{\text{hv}} = 3.21$ eV, the KER peaks around 0.5 eV [7], resulting in a recoil velocity $v = 9.7 \times 10^5$ cm/s for H atom and 6.8×10^5 cm/s for D atom, about one order of magnitude larger than those of OH/OD. Using the same procedure described above for OH/OD + CO, $\alpha = 1.4^\circ$ for H atom and 1.9° for D atom are obtained—in other words, the axial recoil approximation is much better for this dissociation channel. However, because the photofragment β_2 parameter was not measured for H/D + CO₂, the function of η versus γ cannot be obtained with the present experimental data. Thus, we will defer a more detailed treatment of the lifetimes in the H/D + CO₂ dissociation channel at this time.

4.3. Photofragment angular distribution in two-photon DPD

Our previous study suggested that the strong two-photon absorption at $E_{\text{hv}} = 1.60$ eV was mediated by a p -type shape resonance near the photodetachment threshold, leading to a significant alignment of the transient HOCO[−] produced by absorption of the first photon. In such a process, the low-energy p -partial wave outgoing electrons are temporarily trapped by a

centrifugal barrier, forming a shape resonance that selects HOCO[−] aligned parallel with laser polarization (consistent with the parallel transition dipole discussed above). The LF angular distribution of the OH + CO neutral photofragments in the two-photon DPD provides the further evidence for this phenomenon. Compared with Figure 3, the LF angular distribution of OH + CO in the two-photon process is more anisotropic along the laser polarization, supported by a larger β_2 (1.3 ± 0.2 in the two-photon process compared with 0.8 ± 0.1 in the one-photon process) and the emergence of a positive β_4 . This observation provides solid evidence for the alignment of HOCO[−] along the laser \vec{E} vector during the two-photon photodetachment as inferred from the LF-PADs presented in [20].

5. Conclusion

In summary, the dynamics of the one ($E_{\text{hv}} = 3.21$ eV) and two-photon ($E_{\text{hv}} = 1.60$ eV) DPD processes, HOCO[−] + $h\nu \rightarrow$ OH + CO + e[−] and HOCO[−] + $h\nu \rightarrow$ H + CO₂ + e[−], have been studied by a measurement of the photoelectron and photofragment energy and angular distributions in coincidence. Examination of the angular correlations among the photoelectron, photofragments, and the laser polarization reveals that the DPD of HOCO[−] is characterized by a transition dipole in the HOCO symmetry plane. Anisotropy parameters for the LF- and RF-PAD, as well as for the LF photofragment angular distribution of the OH + CO products, are reported. With these parameters, the relationship between the HOCO/DOCO lifetime and orientation of transition dipole has been investigated using a classical model. The upper limits of lifetime are reported to be 9×10^{-13} and 1.3×10^{-12} s for HOCO and DOCO radicals dissociating to OH/OD + CO products, respectively, and have been compared with several previous measurements. In addition, the angular distribution measurement in the two-photon DPD of HOCO[−] at $E_{\text{hv}} = 1.60$ eV supports the results of our previous study that the alignment of a molecular anion can be realized through a shape resonance near the photodetachment threshold. Future work employing a higher beam energy (up to 16 keV) to improve the DAF for H/D atoms, as well as measuring the H + CO₂ product angular distribution as a function of different laser polarizations, may help extract a reliable anisotropy parameter for H + CO₂ fragments and yield further insights into the HOCO lifetime and DPD dynamics leading to the production of H + CO₂. Regrettably, detailed electron–molecule scattering dynamics

information is not obtained from the current RF-PAD measurement, due to the HOCO lifetime and the concomitant blurring of the photoelectron-photofragment angular correlations. Further studies, possibly making use of HOCO⁻ alignment by dipole excitation through shape-resonant states, may allow extraction of the photoelectron anisotropy parameters A_i in a frame with the molecular transition dipole spatially aligned along the pump laser polarization [20,36]. These experimental results accompanied by further quantum dynamics calculations should clarify in greater detail the role of the HOCO intermediate on the complicated potential energy surface that governs the fundamental OH + CO → H + CO₂ reaction.

Acknowledgements

This work was supported by the Department of Energy (DOE) under the Grant No. DE-FG03-98ER14879.

References

- [1] R.E. Continetti, *Annu. Rev. Phys. Chem.* **52**, 165 (2001).
- [2] D.M. Neumark, *Phys. Chem. Chem. Phys.* **7**, 433 (2005).
- [3] R.E. Continetti, *Int. Rev. Phys. Chem.* **17**, 227 (1998).
- [4] K.A. Hanold, M.C. Garner, and R.E. Continetti, *Phys. Rev. Lett.* **77**, 3335 (1996).
- [5] K.A. Hanold and R.E. Continetti, *Chem. Phys.* **239**, 493 (1998).
- [6] T.G. Clements, R.E. Continetti, and J.S. Francisco, *J. Chem. Phys.* **117**, 6478 (2002).
- [7] Z. Lu, Q. Hu, J.E. Oakman, *et al.*, *J. Chem. Phys.* **126**, 194305 (2007).
- [8] G.E. Busch and K.R. Wilson, *J. Chem. Phys.* **56**, 3638 (1972).
- [9] K.L. Reid, *Annu. Rev. Phys. Chem.* **54**, 397 (2003).
- [10] E. Surber, R. Mabbs, and A. Sanov, *J. Phys. Chem. A.* **107**, 8215 (2003).
- [11] M.S. Bowen and R.E. Continetti, *J. Phys. Chem. A.* **108**, 7827 (2004).
- [12] O. Gessner, A.M.D. Lee, J.P. Shaffer, *et al.*, *Science* **311**, 219 (2006).
- [13] J.A. Miller, R.J. Kee, and C.K. Westbrook, *Annu. Rev. Phys. Chem.* **41**, 345 (1990).
- [14] T. Rockmann, C.A.M. Brenninkmeijer, G. Saueressig, *et al.*, *Science* **281**, 544 (1998).
- [15] I.W.M. Smith, *Chem. Phys. Lett.* **49**, 112 (1977).
- [16] H.G. Yu, J.T. Muckerman, and T.J. Sears, *Chem. Phys. Lett.* **349**, 547 (2001).
- [17] M.J. Lakin, D. Troya, G.C. Schatz, *et al.*, *J. Chem. Phys.* **119**, 5848 (2003).
- [18] X.L. Song, J.C. Li, H. Hou, *et al.*, *J. Chem. Phys.* **125**, 094301 (2006).
- [19] S. Zhang, D.M. Medvedev, E.M. Goldfield, *et al.*, *J. Chem. Phys.* **125**, 164321 (2006).
- [20] Z. Lu and R.E. Continetti, *Phys. Rev. Lett.* **99**, 113005 (2007).
- [21] J.A. Davies, J.E. LeClaire, R.E. Continetti, *et al.*, *J. Chem. Phys.* **111**, 1 (1999).
- [22] J.A. Davies, R.E. Continetti, D.W. Chandler, *et al.*, *Phys. Rev. Lett.* **84**, 5983 (2000).
- [23] J. Cooper and R.N. Zare, *J. Chem. Phys.* **48**, 942 (1968).
- [24] D. Dill, *J. Chem. Phys.* **65**, 1130 (1976).
- [25] E.P. Wigner, *Phys. Rev.* **73**, 1002 (1948).
- [26] K.J. Reed, A.H. Zimmerman, H.C. Andersen, *et al.*, *J. Chem. Phys.* **64**, 1368 (1976).
- [27] R.N. Zare, *Mol. Photochem.* **4**, 1 (1972).
- [28] R.E. Continetti, D.R. Cyr, and D.L. Osborn, *J. Chem. Phys.* **99**, 2616 (1993).
- [29] T.G. Clements. PhD thesis, University of California, San Diego, 2002.
- [30] J. Cooper and R.N. Zare, in *Lectures in Theoretical Physics* (Gordon and Breach, Inc., New York, 1969), Vol. XI, p. 317.
- [31] Y.M. Li and J.S. Francisco, *J. Chem. Phys.* **113**, 7963 (2000).
- [32] L.B. Harding. unpublished data.
- [33] S.I. Ionov, G.A. Brucker, C. Jaques, *et al.*, *J. Chem. Phys.* **97**, 9486 (1992).
- [34] N.F. Scherer, C. Sipes, R.B. Bernstein, *et al.*, *J. Chem. Phys.* **92**, 5239 (1990).
- [35] M. Brouard, D.W. Hughes, K.S. Kalogerakis, *et al.*, *J. Chem. Phys.* **112**, 4557 (2000).
- [36] T. Suzuki, *Annu. Rev. Phys. Chem.* **57**, 555 (2006).